Solid Freeform Fabrication 2017: Proceedings of the 28th Annual International Solid Freeform Fabrication Symposium – An Additive Manufacturing Conference
Reviewed Paper

Melt Pool Dimension Measurement In Selective Laser Melting Using Thermal Imaging

Bo Cheng[1], James Lydon[2], Kenneth Cooper[2], Vernon Cole[3], Paul Northrop[3], Kevin Chou[1]

[1] Industrial Engineering Department
University of Louisville
Louisville, KY 40292, USA

[2] Additive Manufacturing Laboratory
Marshall Space Flight Center
Huntsville, AL 35812

[3] CFD Research Corporation
Huntsville, AL 35806

Abstract

Process temperature measurement for selective laser melting (SLM) can provide critical information such as melt pool dimension for real-time part quality control. In this study, a MCS640 LumaSense thermal imager was utilized to collect process radiant temperature information during SLM fabrication using Inconel718 powder. Identified liquidus-solidus transition was used to calculate melt pool size. Speed effect on melt pool dimension has been investigated. The major findings are as follows. (1) At a beam power of 180 W, the averaged melt pool has dimensions of about 0.39 mm and 0.23 mm in length and width for 400 mm/s scanning speed. (2) No significant difference has been observed for melt pool size at different build height for a given scanning speed. (3) Melt pool width decreases with the increase of scanning speed, while similar melt pool length was observed at different speed under a laser power of 180 W.

Keywords: Selective Laser Melting (SLM); Infrared Imaging; Melt Pool Size

1. Introduction

Selective Laser Melting (SLM) based on additive layered fabrication can build complex structures such as lattice and internal features. SLM technology utilizes a high energy laser beam to scan predefined cross section; fabricated part quality deficiency such as porosity may be resulted by incomplete melt under different process conditions. To overcome the part quality variance problem, a thorough understanding of real time process thermal characteristics is needed. Thermal imaging technology is utilized to monitor the SLM process, it can successfully capture the transient thermal response. The main part of thermal imaging system is an infrared (IR) camera with special wavelength and frame rate, it is usually used to record build surface temperature distribution in SLM process. However, the thermal camera may not output true temperature measurement results; they usually give radiant temperature information based on material emissivity information. It needs to mention that the material emissivity can vary with temperature, material state (powder/solid/liquid), or camera view angle [1]. Such variances make the accurate measurement of true temperature extremely difficult. Instead of trying to capture true temperature, some of the

comparatively easy-to-identify characteristics of the temperature profile could be utilized to digest useful information from collected data. The liquidus-solidus transition, which is happened during material liquid to solid phase transformation, would cause a sharp change in temperature profile (plateau) due to latent heat of fusion effect. This discontinuity may be used as a threshold point for melt pool dimension measurement [2].

Thermal imaging of temperature information in SLM or selective laser sintering (SLS) has been studied by different researchers. Charge-coupled Device (CCD) camera was utilized to measure the brightness temperature in SLM process by Yadroitsev et al [3], the authors were able to calculate melt pool max true temperature based on measured solidification temperature. An optical temperature monitoring system was developed by Chivel and Smurov [4] for SLS/SLM process. It was possible to optimize SLS powder bed porosity with this developed system based on the obtained spatial distribution of brightness temperature. Gao et al [5] used IR imager to measure the point temperature distribution in SLS process, numerical model was then validated by collected thermal information. However, relatively few studies have been done to measure melt pool dimension by thermal imaging of powder bed process. Heigel and Lane [6] utilized a high speed IR camera (1800 frames per second) to record the thermal information in SLM process. The authors have investigated the effect of different combinations of the laser speed and power on melt pool length when laser beam scanning on a bare In625 plate. The melt pool length was obtained by identifying the liquid-solidus transition discontinuity. Due to observed vapor plume or reflection around the melt pool width direction, no meaningful melt pool width could be reported. Cheng et al [7] have tested thermal imaging measurement for Monel K500 powder material in SLM process. The authors have utilized a MCS640 LumaSense IR camera to collect radiant temperature information at different build height throughout the entire build, under a constant laser power of 180 W and speed of 600 mm/s. The phase transition region of the temperature profiles was utilized to identify melt pool sizes. It was found that the melt pool length was constantly around 0.6 mm at different build height. On the other hand, for powder bed electron beam additive manufacturing (EBAM) process, Chou's group [8, 9] has conducted build surface temperature measurement for Ti64 material using near infrared (NIR) camera, the experimental temperatures and melt pool sizes were compared against the thermal finite element simulations for model validations. In their study, the NIR imager was mounted on a tripod near the EBAM machine's viewport with a vertically inclined angle of ~35 degree; the camera has a spectral range of 0.78–1.08 μm so as to ensure the radiant signal can be captured. The experimental results and numerical simulations have indicated that the melt pool dimensions and part surface morphology were subject to change based on different scanning speed.

Process parameter will strongly affect the melt pool size, which may affect the part quality such as microstructure [10, 11]. Thus, experimentally measurement of process thermal information could provide vital information for next step analysis, such as thermal model validation and process-quality map for build part. The objective of this work is to investigate process parameters effect on the thermal characteristics in SLM process. Experiments were designed and conducted to vary the scanning speed of the Concept Laser M1 machine. Build part surface temperatures were recorded using IR imaging system with data processing by in-house code. Melt pool sizes were analyzed and compared for three different beam speeds.

2. Experimental Methodology

2.1 Experimental Setup

Concept Laser M1 machine was used to fabricate test parts for thermal characteristic measurement purpose. In718 material was used as raw material in this study. An MCS640 LumaSense thermal imager was used to obtain radiant signal in laser scanning process. It has a 640 x 480 pixel focal plane array sensor (amorphous Si based) with a maximum frame rate of 60 Hz. The integration time of the camera is 16 ms, 0.762 ms and 0.036 ms for the low, medium, and high temperature ranges respectively. The spectral range of the camera was about 670 nm wavelength, which makes the camera be able to collect signal through the laser-blocking view glass in Concept Laser machine. The IR imager has been calibrated against Concept Laser view glass by camera manufacturer. The thermal imager has a detectable temperature range from 600 °C to 3000 °C and has been divided to 3 different ranges: low (nominally 1000 – 1281 °C), medium (nominally 1281 – 1720 °C), and high (nominally 1720 – 2500 °C). The thermal camera was mounted on a tripod and set close to view window, directly focusing on the build plate region so as to include all the three parts into field of view. Figure 1 shows the setup of the camera. More detailed camera information can be found in [12].

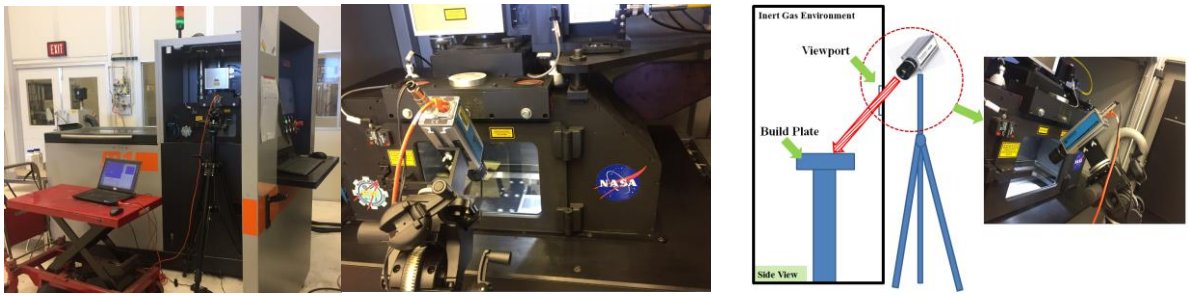

(a) Overview of experimental setup (b) Camera setup

Figure 1. Schematic plot for experimental setup.

The experiment was designed to have better understanding of the speed effect on the melt pool size. The samples were built under the same laser power of 180 W, but each with a different laser scanning speed: 400 mm/s, 600 mm/s and 800 mm/s. Each part had a cross-section of 60 mm length by 5 mm width (in X and Y), and has a height of 25 mm (in Z). The parts were placed with 1 mm distance from each other. Figure 2 shows 3D CAD model with the actual arrangement of the parts during the build. There are two notches on the part with a horizontal distance of 30 mm, which were used for thermal image spatial resolution calculation purpose. The camera field of view is set to cover the region between the notches. To simplify the temperature profile collection along the scanning direction, cross sectional scanning strategy was adapted instead of default chessboard scanning. The scan vector will have a 90^{o} rotation for next layer during building process, e.g., for layer n the laser will scan horizontally with a scan length of 60 mm while for layer n+1 the laser will scan vertically with a scan length of 5 mm. The melt pool measurement will be from vertical scan since there are more scanning tracks to generate statistical data.

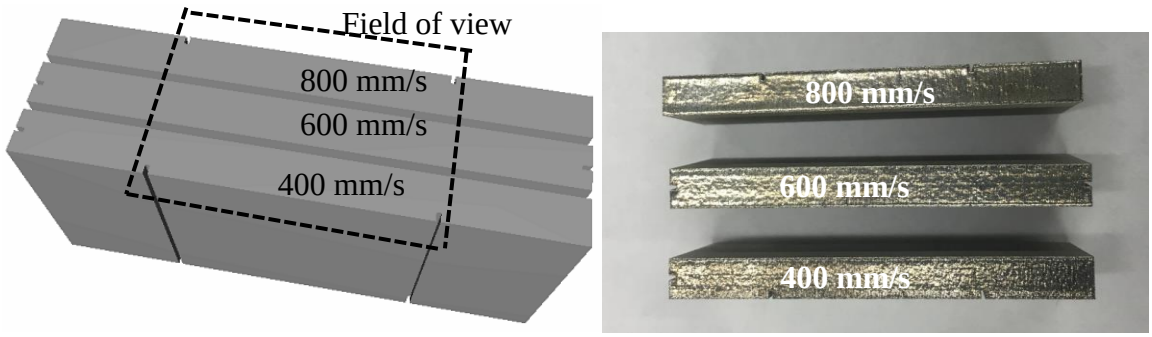

Figure 2. CAD model for different speed scanned samples.

2.2 Typical measurement example

Figure 3 shows examples of collected thermal images during hatch scanning process, collected from three temperature range settings. For this measurement, camera emissivity is set to be 0.3 with a transmission rate of 1.0. Without knowledge of accurate melt pool emissivity, the temperature information shown in Figure 3 is radiant temperature, which is not true temperature. In Figure 3 (a), an elongated cut-off temperature zone (~1600 °C) is shown for low temperature, which may be caused by the interaction of scanning speed and camera integration time (16 ms) at low range setting. The expected high temperature zone followed by a cooling tail can't be acquired by low range camera setting. The motion blur may still be significant for camera medium range setting since the integration time is 0.762 ms. For a high scanning speed such as 800 mm/s, blur area may be captured and lead to melt pool dimension calculation inaccuracy. For the high temperature range image in Figure 3 (c), the integration time is 0.036 ms, which could further reduce the motion blur effect. Thus, it is decided to use high range camera setting for thermal image measurement. It should be mentioned that the minimum temperature from legend bar in Figure 3 only represents the lowest detectable temperature for current IR camera setting; it is not the actual lowest temperature during laser scanning. The actual frame rate during testing is about 58 Hz.

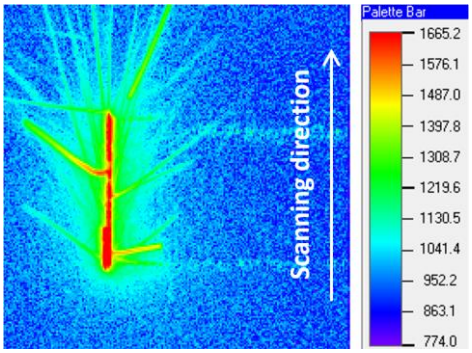

(a) Low range image

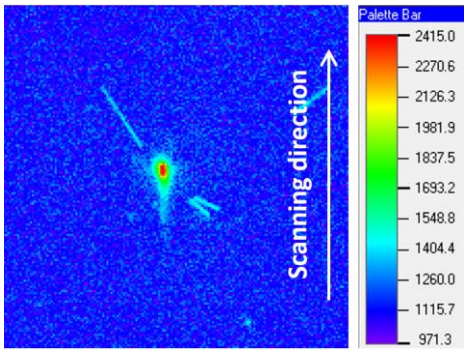

(b) Medium range image

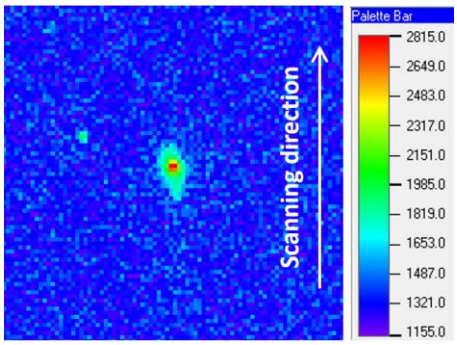

(c) High range image

Figure 3. Typical example of three temperature ranges at 400 mm/s speed (emissivity=0.3, transmission=1.0).

2.3 Spatial resolution and hatch spacing calculation

The spatial resolutions of the thermal images are needed for melt pool dimension analysis. The horizontal and vertical resolutions were calculated based on the part width and the distance between specially designed build notches. There may be perspective distortion caused by the angle of the imager in different locations of the thermal image, thus the resolution will be calculated based on average measurement of all three parts. Figure 4 (a) shows the binary image of part periphery, which has been created from multiple contour scanning images collected by camera low range setting. With the knowledge of horizontal notch distance (30 mm) and vertical part width (5 mm), the resolution is calculated to be 55 µm/pixel (vertical) and 47 µm/pixel (horizontal).

To obtain the scanning track hatch spacing, thermal images from certain number of successive scanning path has been collected and converted to binary image. The distance between the identified initial and final scanning tracks of the domain can be used to determine hatch spacing by counting how many scanning tracks inside the selected domain. Figure 4 (b) shows a typical binary image consisted of 48 scanning tracks for 600 mm/s region. The hatch spacing between neighboring tracks is about 103.2 µm with a standard deviation of 2.5 µm.

Fabricated sample surface morphology has been captured by white light interferometer. Individual scanning route can be clearly observed as elevated tracks. Thus, actual hatch spacing can be identified by drawing a line across multiple scanning tracks and counting the distance between peaks, as shown in Figure 5. The hatch spacing is calculated to be 102.7 µm with a standard deviation of 5.3. The image resolution results have been confirmed by obtaining similar hatch spacing value from both thermal image and surface roughness measurement.

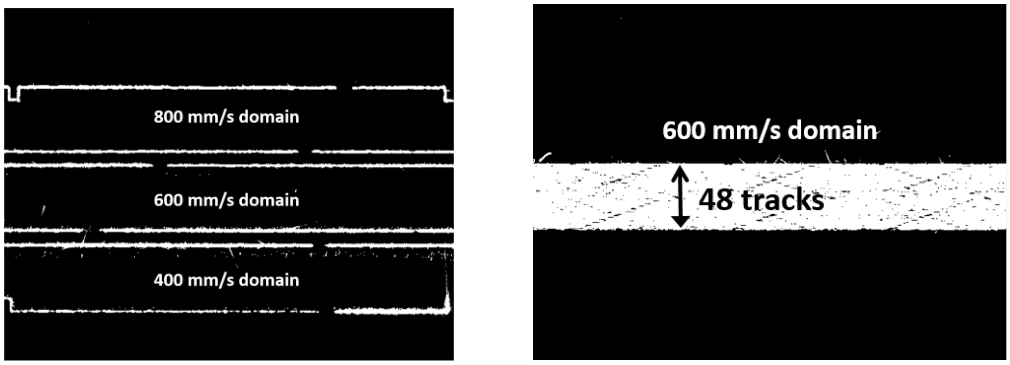

(a) Contour binary image (b) Hatch scanning binary image

Figure 4. Binary image used for resolution and hatch spacing calculation.

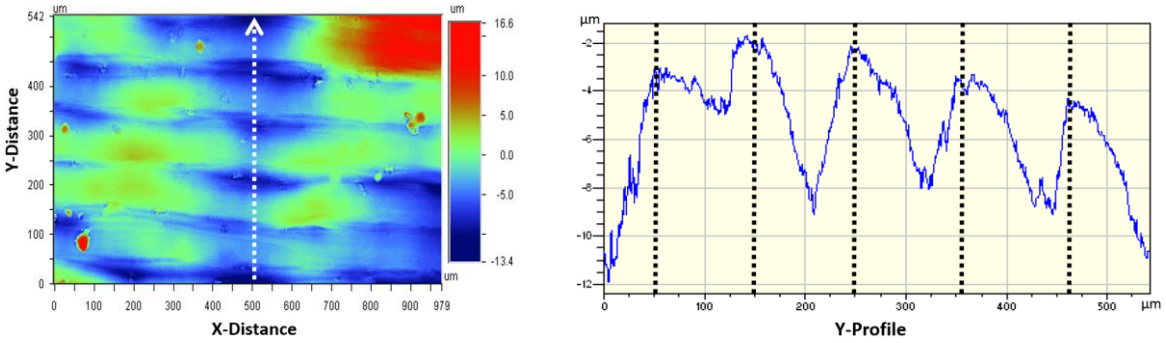

Figure 5. Typical example of hatch spacing calculation.

2.4 Identification of liquidus-solidus transition

In this study, the melt pool dimension will be measured using the liquidus-solidus transition location. However, it is impossible to measure the true temperature of melt pool since the emissivity is unknown for In718 at elevated temperature. Thus, using the literature liquidus-solidus value (1336 – 1260 ^{o}C [13]) to identify melt pool dimension from collected thermal image is inaccurate. A higher emissivity setting of the IR camera would lead to a lower radiant temperature in the thermal image, while a lower emissivity setting of the IR camera can cause higher collected radiant temperature. It is critical to keep the liquidus-solidus transition between upper and lower limitation of camera detectable range. A high emissivity setting may bring the liquidus-solidus transition region to the lower detectable limitation, which is a quite noisy region, thus affecting the liquidus-solidus transition identification. In addition, camera transmission rate setting can also affect the collected temperature magnitude. Without the knowledge of melt pool emissivity, it would be risky to use one set of emissivity and transmission value to collect thermal information throughout the build. The inappropriate emissivity or transmission rate would cause the failure of whole experiment. Thus, different combinations of emissivity and transmission values were tried in the camera. Table 1 shows the camera setting information for different build height. Ideally, the change of emissivity and transmission would only shift the radiant temperature profile up and down; it will not affect the melt pool dimension.

Table 1. IR camera emissivity and transmission setting.

Case No.	1	2	3	4	5	6	7	8	9	10	11
Height(mm)	4.28	4.48	4.62	6.12	6.36	7.96	8.2	8.32	10.16	14.32	14.6
Emissivity	0.3	0.2	1	0.3	1	0.3	1	0.3	0.3	0.3	1
Transmission	1	1	1	1	1	1	1	0.5	1	1	1

Figure 6 shows the collected radiant temperature profile along scanning direction from a typical laser scanning image. A noisy region is shown when temperature drops below 1600 ^{o}C (close to lower limitation of the camera), as shown in Figure 6 (b). The markers have been added to temperature plot to indicate every camera pixel used for the profile. There is a discontinuity in the cooling portion of the temperature profile. The presence of this discontinuity relates to the liquidus-solidus transition and can be used for melt pool dimension calculation; it can be applied in temperature profile in scanning direction for melt pool length calculation and transverse direction for melt pool width calculation. Heigel and Lane [6] developed an algorithm to better identify the discontinuity: The minimum of the 2nd derivative of each pixel of the temperature profile has been calculated to locate the discontinuity; the 2nd derivatives of each pixel are obtained from a 3rd order polynomial which is fitted by one pixel and its 4 closest neighboring pixels (5 total pixels). The same method has been used in this study to identify discontinuity from all collected thermal profiles. Figure 7 shows the detailed process of discontinuity identification: (1) Original temperature profile will be re-aligned according to the max temperature point; (2) interpolation of temperature values between neighboring pixels is needed since it is observed that there are few pixels around the discontinuity area, more temperature points would also help to generate the 3rd order polynomial equation; (3) calculate the minimum of the 2nd derivative for the temperature curve; (4) locate the temperature for discontinuity.

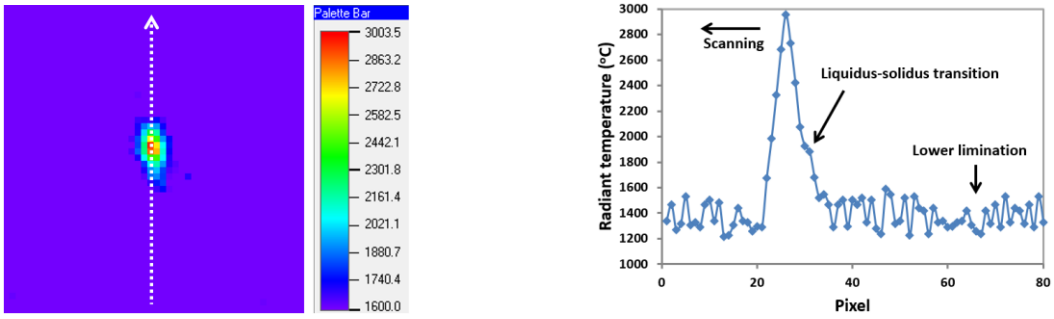

(a) Contour image (b) Radiant temperature (scanning direction)

Figure 6. Example of temperature profile along scanning direction showing the discontinuity for liquidus-solidus transition.

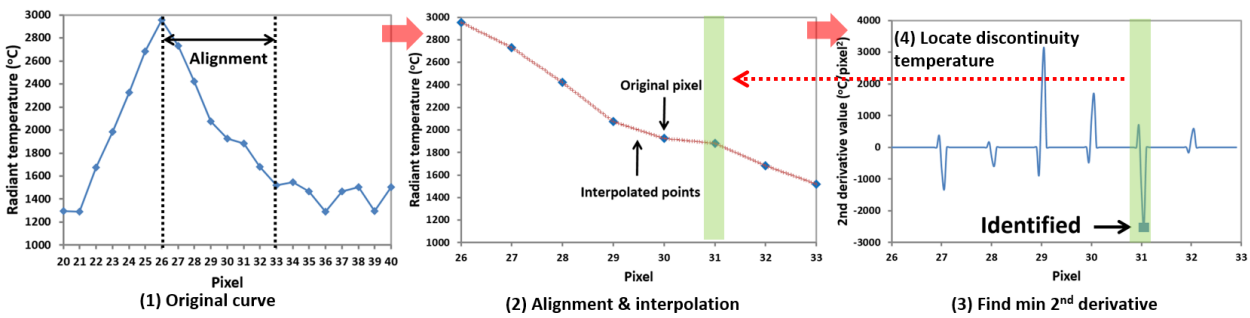

Figure 7. Example of discontinuity identification process.

3. Results and Discussion

3.1 Typical example of radiant temperature profile and melt pool size

Figure 8 shows example of IR images, collected 2D process temperature profile along scanning direction and melt pool dimension. In each image, the laser scans from bottom to top along the white dotted centerline in Figure 8 (a). These thermal images show typical temperature contours under moving laser beam source: a high temperature zone near the laser center and gradually cools down behind the melt pool as the laser moves away. The radiant temperature profiles along scanning track have been extracted and used to analyze liquidus-solidus discontinuity location. The threshold values (discontinuity) for melt pool dimension calculation are: 1890 ^{o}C (400 mm/s), 1855 ^{o}C (600 mm/s) and 1912 ^{o}C (800 mm/s), as shown in Figure 8 (b). These values are fairly close indicating the discontinuity temperature should be similar for a specific build height. Ideally, the phase change temperature should be in a fixed temperature range; however, the radiant temperature would be affected by the relative angle between melt pool surface and thermal camera. Thus, variance in discontinuity temperature may be expected. Melt pool dimensions (white region) are shown in Figure 8 (c), based on identified threshold values. The results show that the 400 mm/s case has a melt pool length of 0.46 mm and a width of 0.21 mm while the 800 mm/s case has a length of 0.4 mm and a width of 0.19 mm. In addition, Figure 8 (a) clearly shows droplet ejected from melt pool. The droplet ejection phenomenon is quite common for 400 mm/s and 600 mm/s scanning speed, while there is only a few for 800 mm/s scanning speed. Lane et al [14] also noticed there could be hot particles ejected from melt pool in SLM process. Moreover, Ly et al [15] pointed out that the velocity of liquid ejections could be as high as 6~20 m/s.

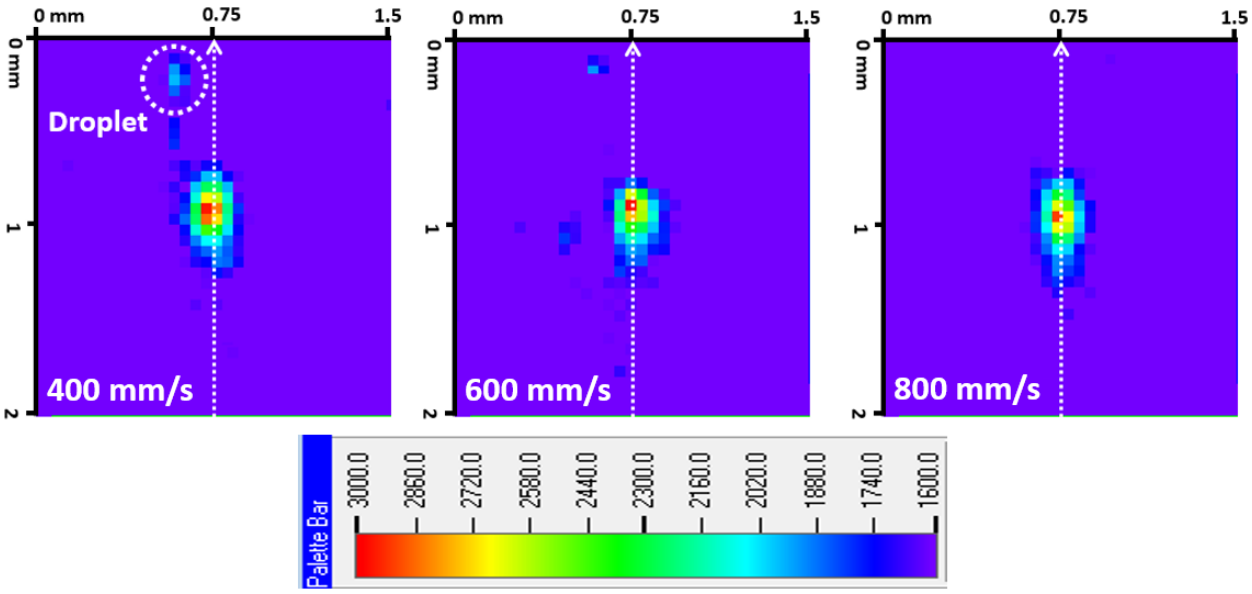

(a) IR images for different scanning speed

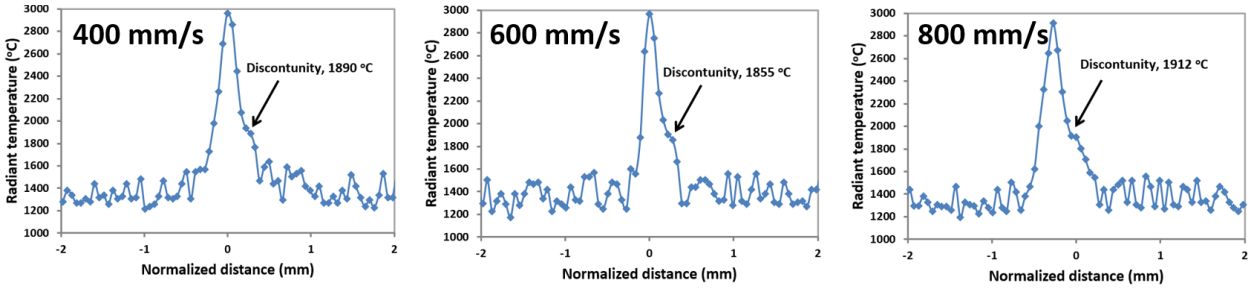

(b) Radiant temperature profile along scanning direction

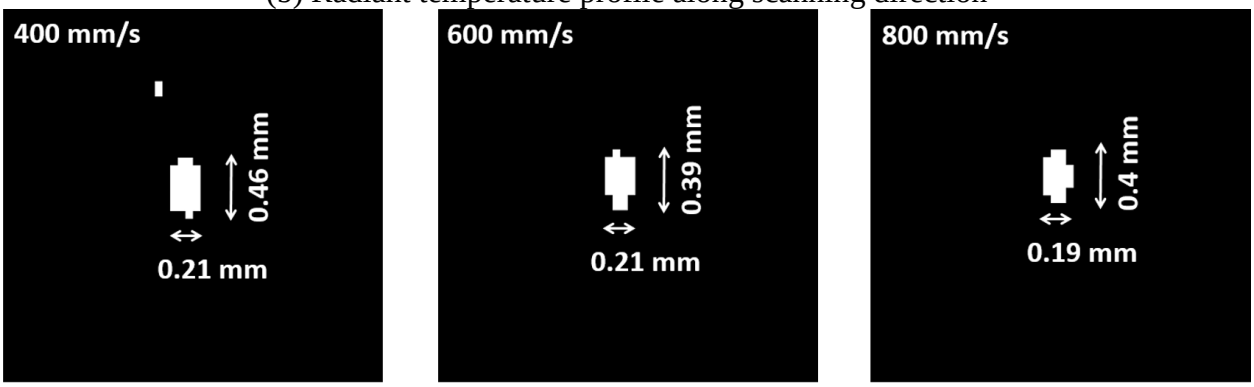

(c) Binary images indicating melt pool using identified discontinuity value

Figure 8. Typical thermal images for different scanning speed.

3.2 Speed effect on melt pool size

Typical examples, from 400 mm/s to 800 mm/s cases, has been analyzed for the relationship between melt pool dimensions and build height, as shown in Figure 9. All the melt pool dimensions have been calculated from multiple frames in one build surface at specific build height. No clear trend was observed for the melt pool size against build height. It may be because that the part can cool down to environmental temperature during the dwelling time between two consecutive layers, thus the residual heat effect for upcoming layer is minimum. The averaged melt pool dimensions, based on multiple layers, have been concluded in Figure 10. Clear decreasing trend is noted for melt pool width when the scanning speed increases, which is caused by the decrease of beam energy density at higher speed. The melt pool width decreases with from 0.23 mm (400 mm/s) to 0.2 mm (800 mm/s). However, the trend in length is unclear for the change of speed. The average length of all build height shows that the melt pool length of 400 mm/s (0.39 mm) is larger than that of 600 mm/s (0.36 mm) and 800 mm/s (0.37 mm), but the length increases slightly when speed changes from 600 mm/s to 800 mm/s. The minor melt pool length increase from 600 mm/s to 800 mm/s may be because of the motion blur effect, especially considering the speed difference (200 mm/s) and the camera integration time of 0.036 ms. In fact, the three scanning speeds have close melt pool length considering the error range. Similar observation has been found in literature [6] that no significant difference of melt pool length was reported when laser speed changed from 200 mm/s to 800 mm/s under a laser power of 195 W for In625.

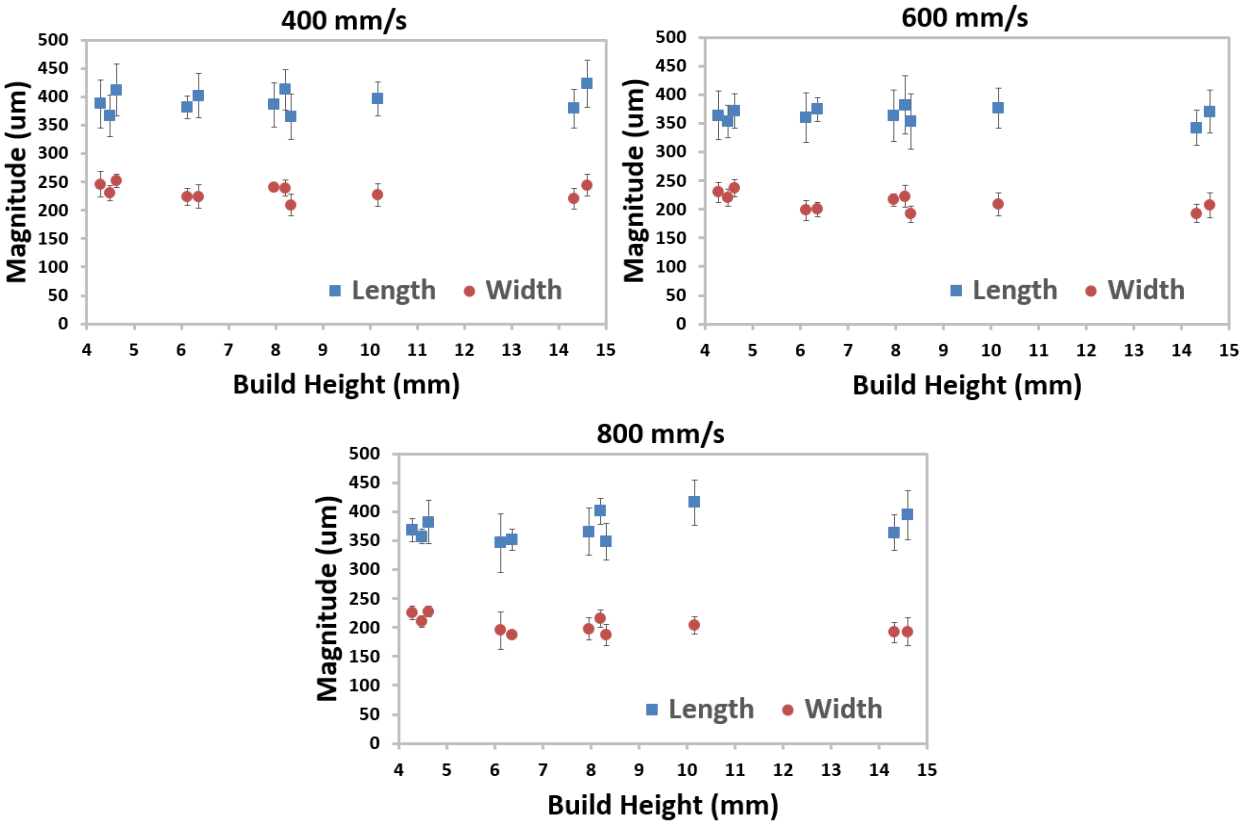

Figure 9. Melt pool dimensions at different build height.

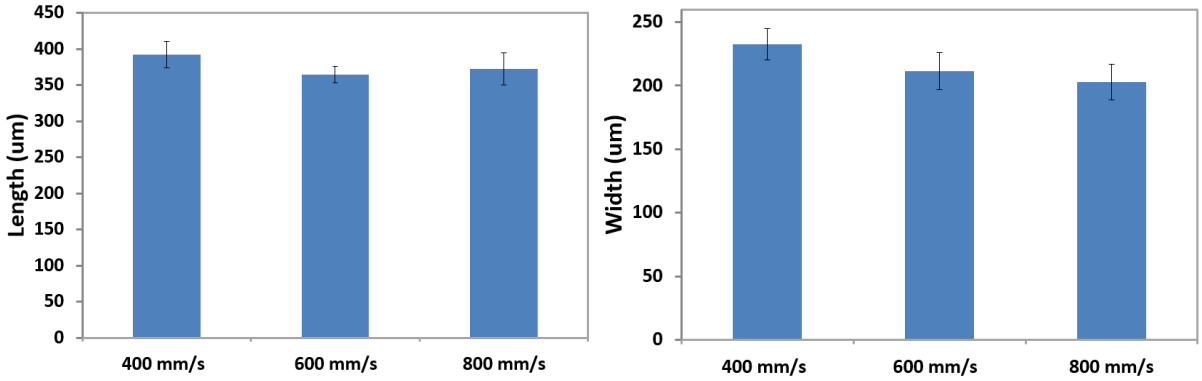

Figure 10. Averaged melt pool dimension for different scanning speed.

4. Conclusion

In this study, IR camera has been utilized to measure melt pool dimensions of In718 material in SLM process. User-designed CAD model was fabricated with special model features to acquire spatial resolution. Speed effect on melt pool dimensions has been studied. The testing results indicated that IR camera was able to capture melt pool characteristics using appropriate setting. The major findings can be summarized as follows:

1. At a beam power of 180 W, the melt pool has average dimensions of about 0.39 mm and 0.23 mm in length and width for 400 mm/s scanning speed, while the dimensions would be 0.37 mm and 0.2 mm in length and width when scanning speed is 800 mm/s.

2. The obtained melt pool length and width has no clear relationship with the change of build height, consistent melt pool dimensions for different speed cases have been observed throughout the build.

3. Melt pool width would decrease with the increase of scanning speed while the trend for length is unclear. Similar melt pool length was observed at different scanning speed under a laser power of 180 W.

Acknowledgment

This research is supported by CFD Research Corp. through a NASA STTR Phase II project. Helpful discussion with Jarred C. Heigel is acknowledged.

Reference

[1] Moylan, S., Whitenton, E., Lane, B., and Slotwinski, J., "Infrared thermography for laser-based powder bed fusion additive manufacturing processes," Proc. AIP Conference Proceedings, AIP, pp. 1191-1196.
[2] Doubenskaia, M., Pavlov, M., Grigoriev, S., and Smurov, I., 2013, "Definition of brightness temperature and restoration of true temperature in laser cladding using infrared camera," Surface and Coatings Technology, 220, pp. 244-247.
[3] Yadroitsev, I., Krakhmalev, P., and Yadroitsava, I., 2014, "Selective laser melting of Ti6Al4V alloy for biomedical applications: Temperature monitoring and microstructural evolution," Journal of Alloys and Compounds, 583, pp. 404-409.
[4] Chivel, Y., and Smurov, I., 2010, "On-line temperature monitoring in selective laser sintering/melting," Physics Procedia, 5, pp. 515-521.
[5] Gao, Y., Xing, J., Zhang, J., Luo, N., and Zheng, H., 2008, "Research on measurement method of selective laser sintering (SLS) transient temperature," Optik-International Journal for Light and Electron Optics, 119(13), pp. 618-623.
[6] Heigel, J. C., and Lane, B. M., 2017, "Measurement of The Melt Pool Length During Single Scan Tracks in A Commercial Laser Powder Bed Fusion Process," Proceedings of ASME 2017 International Manufacturing Science and Engineering Conference (MSEC), Los Angeles, CA, June 4-8, 2017, MSEC2017-2942, pp. 575-591.
[7] Cheng, B., Cooke, S., and Chou, Y. K., 2017, "Preliminary Testing of Temperature Measurements in Selective Laser Melting," Proceedings of ASME 2017 International Manufacturing Science and Engineering Conference (MSEC), Los Angeles, CA, June 4-8, 2017, MSEC2017-3016.
[8] Cheng, B., Price, S., Lydon, J., Cooper, K., and Chou, K., 2014, "On Process Temperature in Powder-Bed Electron Beam Additive Manufacturing: Model Development and Validation," Journal of Manufacturing Science and Engineering, 136(6), pp. 061018-061018.

[9] Price, S., Cheng, B., Lydon, J., Cooper, K., and Chou, K., 2014, "On Process Temperature in Powder-Bed Electron Beam Additive Manufacturing: Process Parameter Effects," Journal of Manufacturing Science and Engineering, 136(6), pp. 061019-061019.
[10] Beuth, J., Fox, J., Gockel, J., Montgomery, C., Yang, R., Qiao, H., Soylemez, E., Reeseewatt, P., Anvari, A., and Narra, S., "Process mapping for qualification across multiple direct metal additive manufacturing processes," Proc. 24th Annual International Solid Freeform Fabrication Symposium - An Additive Manufacturing Conference, pp. 12-14.
[11] Gockel, J., Beuth, J., and Taminger, K., 2014, "Integrated control of solidification microstructure and melt pool dimensions in electron beam wire feed additive manufacturing of Ti-6Al-4V," Additive Manufacturing, 1, pp. 119-126.
[12] Price, S., 2014, "On Temperature Measurements and Analysis in Electron Beam Additive Manufacturing Using Near Infrared Thermography," Master thesis, The University of Alabama, Tuscaloosa, AL.
[13] Cheng, B., Shrestha, S., and Chou, K., 2016, "Stress and deformation evaluations of scanning strategy effect in selective laser melting," Additive Manufacturing, 12, pp. 240-251.
[14] Lane, B., Moylan, S., Whitenton, E. P., and Ma, L., 2016, "Thermographic measurements of the commercial laser powder bed fusion process at NIST," Rapid prototyping journal, 22(5), pp. 778-787.
[15] Ly, S., Rubenchik, A. M., Khairallah, S. A., Guss, G., and Matthews, M. J., 2017, "Metal vapor micro-jet controls material redistribution in laser powder bed fusion additive manufacturing," Scientific Reports, 7.